Abdominal Radiology (2020) 45:2400–2408
https://doi.org/10.1007/s00261-020-02575-7

HEPATOBILIARY

Imaging features of hepatic inflammatory pseudotumor: distinction from colorectal liver metastasis using gadoxetate disodium-enhanced magnetic resonance imaging

Shintaro Ichikawa[1] · Utaroh Motosugi[1,2] · Tatsuya Suzuki[1] · Tatsuya Shimizu[1] · Hiroshi Onishi[1]

Published online: 28 May 2020

Abstract

Purpose To identify gadoxetate disodium-enhanced MRI features distinguishing hepatic IPT from CLM.

Methods From February 2008 to December 2019, 162 lesions (IPT, $n=31$ and CLM, $n=131$) from 94 patients (mean age 65.1 ± 12.2 years; 65 men and 29 women) were retrospectively assessed for the presence or absence of obscure boundary, rim enhancement on arterial phase (AP), persistent rim enhancement during AP to transitional phase (TP), blood vessel penetration, peritumoral parenchymal enhancement on AP, peritumoral parenchymal hypointensity on hepatobiliary phase (HBP), peritumoral parenchymal hyperintensity on T2-weighted imaging (T2WI), biliary dilatation, central hypointensity with a relatively hyperintense periphery on HBP, peripheral hyperintensity on diffusion-weighted imaging (DWI) and T2WI, and lesion to liver signal intensity ratio ($SIR_{lesion/liver}$) on HBP and DWI. Relevant features for differentiating between ITP and CLM were identified by univariate and multivariate analyses.

Results Univariate analysis revealed significantly higher frequencies of the following features in IPT than CLM: younger age, obscure boundary, blood vessel penetration, central hypointensity with a relatively hyperintense periphery on HBP, higher $SIR_{lesion/liver}$ on HBP, and lower $SIR_{lesion/liver}$ on DWI ($P<0.001-0.035$). Rim enhancement on AP and persistent rim enhancement during AP to TP were significantly more common in CLM than in IPT ($P \leq 0.001$). Multivariate analysis revealed that a central hypointensity with a relatively peripheral hyperintensity on HBP, higher $SIR_{lesion/liver}$ on HBP, and lower $SIR_{lesion/liver}$ on DWI were predictive of IPT ($P=0.003-0.039$).

Conclusion Central hypointensity with a relatively peripheral hyperintensity on HBP and $SIR_{lesion/liver}$ on HBP and DWI may be reliable gadoxetate disodium-enhanced MRI features for distinguishing IPT from CLM.

Keywords Gadoxetate disodium · Inflammatory pseudotumor · Liver · Magnetic resonance imaging · Metastasis

Introduction

Inflammatory pseudotumor (IPT) is an inflammatory-related, benign, non-neoplastic mass composed of infiltration of inflammatory cells, fibrous tissue, and myofibroblasts. It occurs most commonly in the lung and orbit, while hepatic IPT is uncommon [1]. Most previous reports on hepatic IPT are case reports; therefore, the imaging findings of this rare disease remains uncertain. Despite recent progress in imaging studies, it is difficult to differentiate IPT from other focal liver lesions, such as colorectal liver metastases (CLM) [2–4], intrahepatic cholangiocarcinoma [5, 6], or hepatocellular carcinoma [7, 8]. Metastatic liver tumors are more frequently observed than primary liver tumors, those can be from breast cancer, lungs cancer, and colorectal cancer [9]. Among them, CLM is the most common in daily practice. It is difficult to distinguish hepatic IPT from CLM, e.g., CLM is often observed as multiple liver lesions, and hepatic ITP also can be solitary or multiple [10, 11]. It is very important to distinguish IPT from CLM, because treatments for these conditions differ. Optimal treatment for CLM is hepatectomy or chemotherapy, whereas IPT can be managed with antibiotics, nonsteroidal anti-inflammatory drugs, steroids, or without medication.

✉ Utaroh Motosugi
umotosugi@nifty.com

[1] Department of Radiology, University of Yamanashi, 1110 Shimokato, Chuo-shi, Yamanashi 409-3898, Japan

[2] Department of Diagnostic Radiology, Kofu Kyoritsu Hospital, Kofu, Japan

Gadoxetate disodium is a liver-specific contrast agent that allows both dynamic studies and liver-specific hepatocyte imaging (hepatobiliary phase [HBP]). Recently, gadoxetate disodium has come to be widely used for liver magnetic resonance imaging (MRI) in daily clinical practice, because of its high performance in lesion detection and characterization [12–14]. However, very few studies have discussed the imaging features of ITP on gadoxetate disodium MRI [15], and to the best of our knowledge, a comparison of the gadoxetate disodium MRI findings between IPT and CLM has not been reported to date. Thus, the purpose of this study was to identify imaging features on gadoxetate disodium-enhanced MRI for distinguishing IPT from CLM.

Materials and methods

Patients

This single-center, retrospective, cross-sectional study was approved by the relevant institutional review board, who waived the requirement for obtaining written informed patient consent due to the retrospective nature of the study. Patients meeting the following inclusion criteria were enrolled between February 2008 and December 2019: (i) availability of gadoxetate disodium-enhanced MRI data, (ii) presence of IPT or CLM with pathological confirmation or clinical diagnosis (IPT: decreased in size on follow-up examinations or after steroid therapy; CLM: increased in size or number on follow-up examinations, or decreased in size after chemotherapy), (iii) lesion size ≥ 10 mm in diameter, and (iv) age ≥ 20 years. To evaluate the differential features of IPT from CLM on gadoxetate disodium-enhanced MRI, all cases who met the inclusion criteria were enrolled because of the rarity of IPT. However, of the 122 patients enrolled for the study, 28 patients were excluded because: (i) diffuse or innumerable metastases were present (23 patients), (ii) images were unevaluable (5 patients). In cases of patients with multiple lesions, the largest 3 lesions were selected for analysis. Therefore, the final study cohort consisted of 94 nonconsecutive patients (mean age, 65.1 ± 12.2 [range 25–87] years), with 162 confirmed liver lesions (Fig. 1). This group included 65 men (64.2 ± 12.1 [25–84] years) and 29 women (67.1 ± 12.4 [41–87] years).

MRI protocols

MRI was performed using a superconducting magnet scanner operated at 1.5 T (Discovery 750; GE Medical Systems, Waukesha, WI, USA) or 3 T (Discovery 750; GE Medical Systems, Waukesha, WI, USA) with an 8- or a 32-channel phased-array coil, respectively. Dynamic studies had been obtained at 20–30 s (arterial phase [AP], scan timing was adjusted using the fluoroscopic triggering technique), and 1 (portal venous phase [PVP]), 2 (transitional phase [TP]), and 20 min (HBP) after administration of gadoxetate disodium. The contrast material (0.025 mmol/kg body weight) had been administered as an intravenous bolus at a rate of 1 mL/s, followed by flushing with 20 mL saline, using a power injector. T2-weighted images (T2WI) and diffusion-weighted images (DWI) were obtained between the TP and HBP. Table 1 presents the MRI parameters in detail.

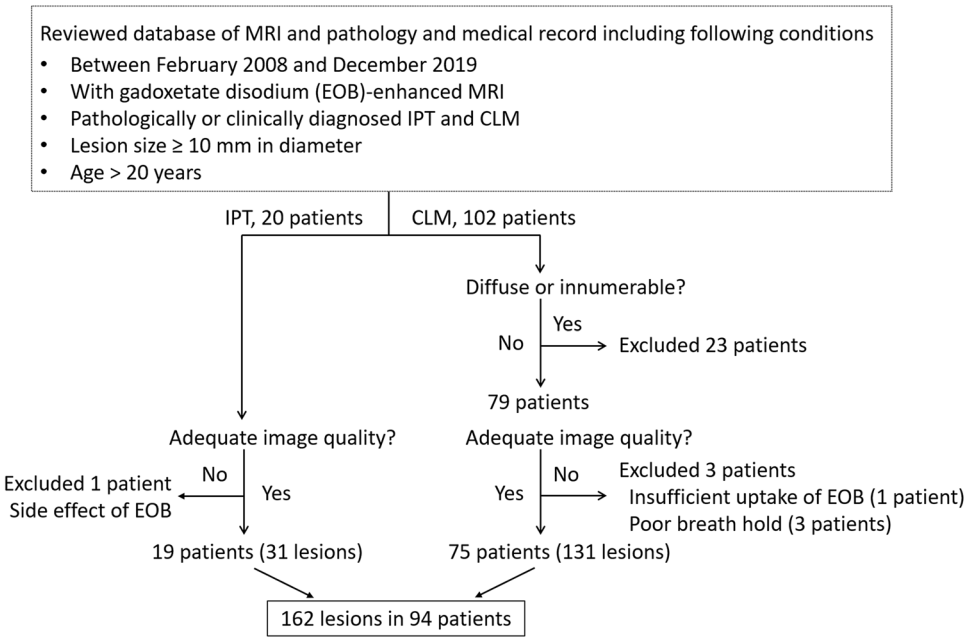

Fig. 1 Flowchart of patient enrollment. *MRI* magnetic resonance imaging, *IPT* inflammatory pseudotumor, *CLM* colorectal liver metastasis

Table 1 Sequence parameters for magnetic resonance imaging

	1.5 T	3 T
Fat-saturated T2-weighted imaging		
Sequence	2D fast spin echo	2D fast spin echo
Repetition time (ms)	Variable (respiratory trigger)	Variable (respiratory trigger)
Echo time (ms)	72	94
Matrix	256 × 192	320 × 320
Section thickness (mm)	6	5
Diffusion-weighted imaging		
Sequence	2D spin echo-EPI	2D spin echo-EPI
Repetition time (ms)	Variable (respiratory trigger)	Variable (respiratory trigger)
Echo time (ms)	64.7	59.7
b value (s/mm^2)	1000	1000
Matrix	128 × 128	128 × 160
Section thickness (mm)	6	6
Contrast-enhanced MRI		
Sequence	3D LAVA	3D LAVA
Repetition time (ms)	3.9	4.8
Echo time (ms)	1.9	2.0
Matrix	320 × 192	320 × 192
Section thickness/intersection gap (mm)	5/-2.5	3.6/-1.8
Flip angle (degree)	12	12
Scan delay after administration	20–30 s, 1, 2, and 20 min	20–30 s, 1, 2, and 20 min

EPI echo planar imaging, *LAVA* liver acquisition with volume acceleration

Image analysis

All data, including the MRI findings, clinical information, and pathological records were collected for all patients by the study coordinator (anonymized, with 4 years of experience in abdominal radiology), who attempted to determine the size and location of the IPT and CLM lesions on MRI. Then, 2 radiologists (anonymized), with 11 and 5 years of experience in liver imaging, independently assessed MR images. They were unaware of the clinical information or final diagnosis. The following findings were evaluated for the presence or absence of the following: obscure boundary, rim enhancement on AP, persistent rim enhancement during AP to TP, blood vessel penetration, peritumoral parenchymal enhancement on AP, peritumoral parenchymal hypointensity on HBP, peritumoral parenchymal hyperintensity on T2WI, bile duct dilatation, central hypointensity with a relatively peripheral hyperintensity on HBP, peripheral hyperintensity on DWI, and peripheral hyperintensity on T2WI (Fig. 2). The signal intensity (SI) of the liver and lesion were measured on HBP and DWI. The SI ratio of the lesion to the liver ($SIR_{lesion/liver}$) was calculated as follows:

$$SIR_{lesion/liver} = SI_{lesion} / SI_{liver}$$

where, SI_{lesion} and SI_{liver} are the SI values for the lesion and the liver, respectively. For quantitative analysis, the largest possible regions of interest were placed on the lesion and liver, away from necrotic areas or large vessels.

Statistical analysis

Analyses were performed for all lesions included in this study and size-matched cases in which 3 CLM lesions were randomly selected to correspond to each IPT lesion. For univariate analysis, categorical variables were compared between IPT and CLM using the Chi-squared test, whereas continuous variables were compared using the Wilcoxon test. For multivariate analysis, the odds ratio was estimated by logistic regression analysis using variables that were identified as significant for distinguishing between IPT and CLM by univariate analysis. The discriminative capacities of $SIR_{lesion/liver}$ on HBP and DWI were assessed using receiver operating characteristic (ROC) curve analysis. The optimal cutoff value was determined; then, sensitivity, specificity, positive- and negative-likelihood ratios, and the area under the ROC curve (AUC) were calculated to differentiate between IPT and CLM for all cases. Cohen's kappa values (κ) or intraclass correlation coefficients (ICCs; r) were calculated to assess interobserver agreement. Agreement was considered excellent for κ or $r > 0.8$, good for $0.6 < \kappa$ or $r \leq 0.8$, moderate for $0.4 < \kappa$ or $r \leq 0.6$, fair for $0.2 < \kappa$ or $r \leq 0.4$, and poor for κ or $r \leq 0.2$. All statistical analyses were performed using JMP software (version 15.0.0; SAS Institute Inc.,

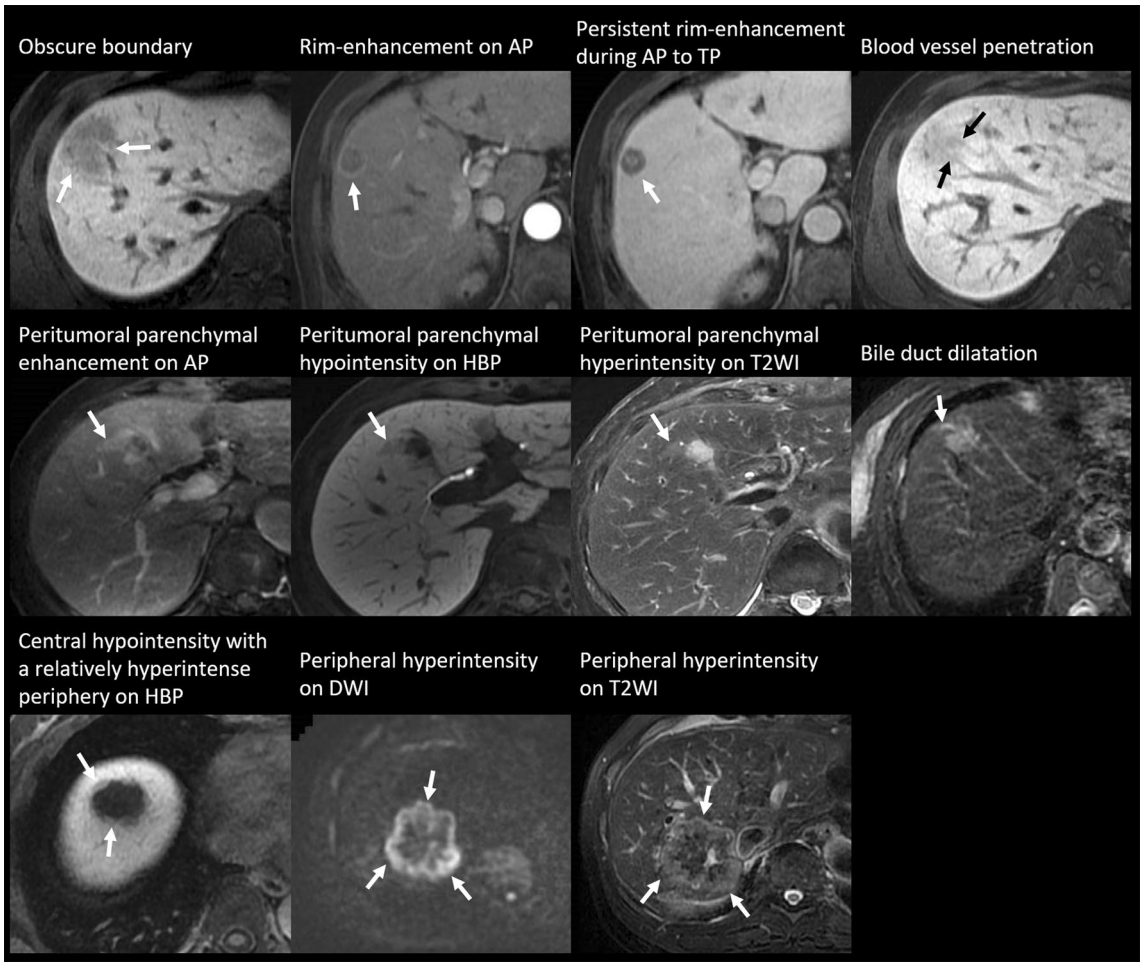

Fig. 2 Examples of magnetic resonance images with visual assessment. *AP* arterial phase, *TP* transitional phase, *HBP* hepatobiliary phase, *T2WI* T2-weighted image, *DW* diffusion-weighted image

Cary, NC, USA). *P*-values < 0.05 were considered statistically significant.

Results

Lesion characteristics

Final diagnosis of 162 liver lesions were as follows: IPT, $n = 31$, mean size, 19.6 ± 12.3 (range 10–58) mm) and CLM, $n = 131$, 22.4 ± 12.6 (10–70) mm. Of the 31 lesions, 7 IPT lesions were pathologically confirmed, while 24 IPT lesions were clinically diagnosed. On the other hand, 46 CLM lesions had pathological confirmation, while 85 CLM lesions were clinically diagnosed. Ninety-three CLM lesions were selected as size-matched cases (19.6 ± 12.0 [10–65] mm). Of these 93 CLM lesions, 33 lesions were pathologically confirmed, while 60 lesions were clinically diagnosed.

Univariate analysis

There were significant differences between IPT and all CLM cases in terms of age (IPT vs. CLM, mean, 59.3 vs. 66.5 years), obscure boundary (23/31 [74.2%] vs. 28/131 [21.4%]), rim enhancement on AP (9/31 [29.0%] vs. 110/131 [84.0%]), persistent rim enhancement during AP to TP (1/31 [3.2%] vs. 39/131 [29.8%]), blood vessel penetration (14/31 [45.2%] vs. 2/131 [1.5%]), central hypointensity with a relatively hyperintense periphery on HBP (12/31 [38.7%] vs. 6/131 [4.6%]), and $SIR_{lesion/liver}$ on HBP (mean, 0.63 vs. 0.45) and DWI (mean, 2.02 vs. 3.57) ($P < 0.001$–0.035, Table 2, Fig. 3). In the comparison between IPT and size-matched CLM lesions, age (mean, 59.3 vs. 66.6 years), obscure boundary (23/31 [74.2%] vs. 14/93 [15.1%]), rim enhancement on AP (9/31 [29.0%] vs. 74/93 [79.6%]), persistent rim enhancement during AP to TP (1/31 [3.2%] vs. 24/93 [25.8%]), blood vessel penetration (14/31 [45.2%] vs. 2/93 [2.2%]), central hypointensity with a relatively

Table 2 Univariate analysis and interobserver agreement of IPT vs. CLM

Variables	IPT ($n=31$ in 19 patients)	All cases ($n=131$ in 75 patients)		Size matched cases ($n=93$ in 63 patients)		Interobserver agreement
		CLM	*P* value (vs. IPT)	CLM	*P* value (vs. IPT)	
Age (years)	59.3 ± 13.6	66.5 ± 11.4	0.035*	66.6 ± 12.0	0.031*	–
Sex (men:women)	11:8	54:21	0.271	44:19	0.406	–
Body weight (kg)	58.8 ± 10.9	60.3 ± 10.5	0.738	59.0 ± 10.2	0.969	–
Chronic liver disease	21.1% (4/19)	12.0% (9/75)	0.291	14.3% (9/63)	0.486	–
Size (mm)	19.6 ± 12.3	22.4 ± 12.6	0.103	19.7 ± 12.0	0.777	–
Obscure boundary	74.2% (23/31)	21.4% (28/131)	< 0.001*	15.1% (14/93)	< 0.001*	0.696 (0.567–0.826)
Rim enhancement on AP	29.0% (9/31)	84.0% (110/131)	< 0.001*	79.6% (74/93)	< 0.001*	0.800 (0.704–0.896)
Persistent rim enhancement during AP to TP	3.2% (1/31)	29.8% (39/131)	0.001*	25.8% (24/93)	0.005*	0.678 (0.565–0.790)
Blood vessel penetration	45.2% (14/31)	1.5% (2/131)	< 0.001*	2.2% (2/93)	< 0.001*	0.534 (0.305–0.763)
Peritumoral parenchymal enhancement on AP	29.0% (9/31)	23.7% (31/131)	0.643	24.7% (23/93)	0.641	0.652 (0.523–0.782)
Peritumoral parenchymal hypointensity on HBP	19.4% (6/31)	19.1% (25/131)	1.000	23.7% (22/93)	0.805	0.745 (0.626–0.865)
Peritumoral parenchymal hyperintensity on T2WI	32.3% (10/31)	19.1% (25/131)	0.144	19.4% (18/93)	0.145	0.636 (0.490–0.781)
Bile duct dilatation	6.5% (2/31)	5.4% (7/131)	0.683	7.5% (7/93)	1.000	0.511 (0.195–0.826)
Central hypointensity with a relatively peripheral hyperintensity on HBP	38.7% (12/31)	4.6% (6/131)	< 0.001*	2.2% (2/93)	< 0.001*	0.718 (0.520–0.916)
Peripheral hyperintensity on DWI	19.4% (6/31)	38.2% (50/131)	0.059	36.6% (34/93)	0.082	0.734 (0.631–0.837)
Peripheral hyperintensity on T2WI	19.4% (6/31)	26.7% (35/131)	0.494	25.8% (24/93)	0.629	0.781 (0.671–0.891)
$SIR_{lesion/liver}$ on HBP	0.63 ± 0.11	0.45 ± 0.08	< 0.001*	0.45 ± 0.09	< 0.001*	0.726 (0.644–0.791)
$SIR_{lesion/liver}$ on DWI	2.02 ± 0.80	3.57 ± 1.06	< 0.001*	3.70 ± 1.10	< 0.001*	0.660 (0.564–0.739)

Continuous variables were analyzed by Wilcoxon test and are expressed as mean ± standard deviation. Categorical variables were analyzed by the χ^2 test and are expressed as percentage with numerators and denominators. Interobserver agreement are presented with the 95% confidence interval in parentheses

IPT inflammatory pseudotumor, *CLM* colorectal liver metastasis, *AP* arterial phase, *TP* transitional phase, *HBP* hepatobiliary phase, *T2WI* T2-weighted image, *DWI* diffusion-weighed image, $SIR_{lesion/liver}$ signal intensity ratio of lesion to liver

*$P < 0.05$

hyperintense periphery on HBP (12/31 [38.7%] vs. 2/93 [2.2%]), and $SIR_{lesion/liver}$ on HBP (mean, 0.63 vs. 0.45) and DWI (mean, 2.02 vs. 3.70) showed significant differences between the groups ($P < 0.001$–0.031. Table 2).

Interobserver agreement

Interobserver agreement of all items was moderate to excellent (κ or $r = 0.511$–0.800), with most showing moderate agreement (Table 2).

Multivariate analysis

Multivariate analysis revealed that central hypointensity with a relatively hyperintense periphery on HBP (Odds ratio [95% confidence interval] for versus all CLM and size-matched CML, 585.5 [8.461–4.052×10^4] and 850.0 [15.56–4.642×10^4]), higher $SIR_{lesion/liver}$ on HBP (1.382×10^{10} [3.255–5.870×10^{19}] and 1.157×10^7 [60.51–2.210×10^{12}]), and lower $SIR_{lesion/liver}$ on DWI (0.083 [0.009–0.758] and 0.117 [0.027–0.502]) favored IPT over CLM in the comparison between IPT and all CLM cases ($P = 0.003$–0.039) and between IPT and size-matched CLM lesions ($P = 0.001$–0.009, Table 3).

ROC curve analysis

The discrimination ability of $SIR_{lesion/liver}$ on HBP and DWI are shown in Table 4. According to ROC curve analysis, the AUCs of $SIR_{lesion/liver}$ on HBP and DWI for the differentiation between IPT and CLM were both high (0.895 and 0.907,

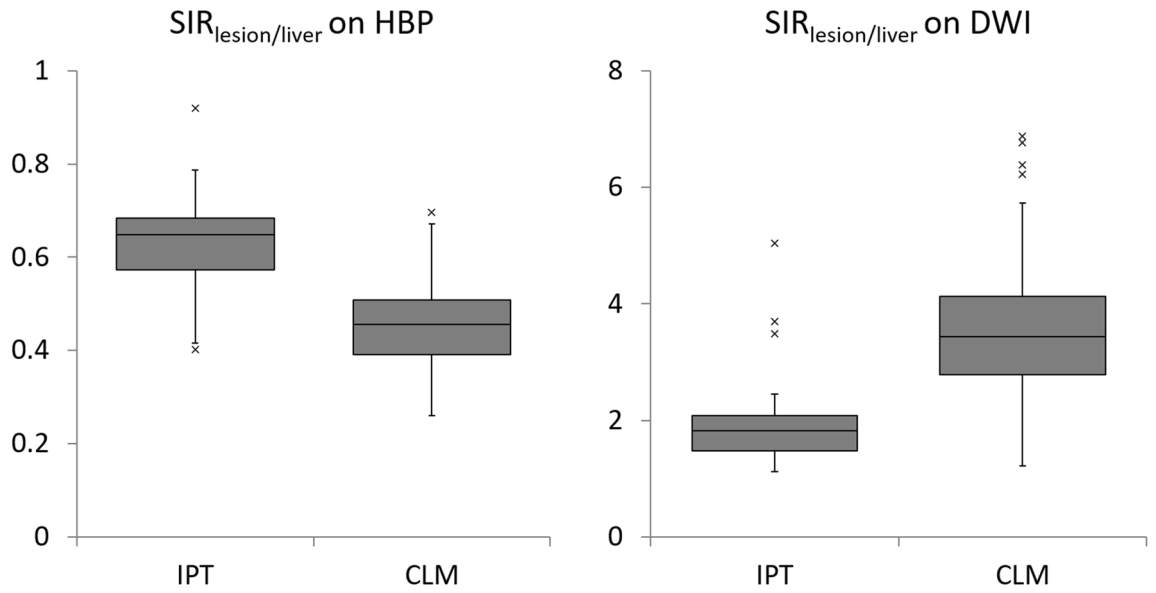

Fig. 3 Boxplot of signal intensity ratio of the lesion to liver. (Left) Signal intensity ratio of the lesion to liver ($SIR_{lesion/liver}$) on hepatobiliary phase (HBP). (Right) $SIR_{lesion/liver}$ on diffusion-weighted imaging (DWI). $SIR_{lesion/liver}$ on HBP of inflammatory pseudotumor (IPT) (median 0.65) was higher than that of colorectal liver metastasis (CLM) (median 0.45; $P < 0.001$). $SIR_{lesion/liver}$ on DWI of IPT (median 1.82) was lower than that of CLM (median 3.44; $P < 0.001$). *Note* In the boxplots, the box indicates from the first quartile (Q1) to the third quartile (Q3). The horizontal line within the box indicates the median of the dataset. The vertical lines indicate Q1–1.5 × IQR (interquartile range) and Q3 + 1.5 × IQR. Cross marks indicate outliers

Table 3 Multivariate analysis for distinguishing IPT from CLM

Variables	All cases		Size matched cases	
	Odds ratio (IPT vs. CLM)	*P* value	Odds ratio (IPT vs. CLM)	*P* value
Age	0.925 (0.797–1.074)	0.306	0.954 (0.886–1.026)	0.203
Obscure boundary	3.726×10^5 (0–NA)	0.999	5.935×10^5 (0–NA)	0.996
Rim enhancement on AP	0.133 (0.009–2.080)	0.151	0.449 (0.065–3.089)	0.416
Persistent rim enhancement during AP to TP	0.995 (0.032–30.54)	0.998	0.290 (0.011–7.952)	0.464
Blood vessel penetration	9.566 (5.330×10^{-12}–1.717×10^{13})	0.875	14.03 (0.001–1.835×10^5)	0.585
Central hypointensity with a relatively peripheral hyperintensity on HBP	585.5 (8.461–4.052×10^4)	0.003*	850.0 (15.56–4.642×10^4)	0.001*
$SIR_{lesion/liver}$ on HBP	1.382×10^{10} (3.255–5.870×10^{19})	0.039*	1.157×10^7 (60.51–2.210×10^{12})	0.009*
$SIR_{lesion/liver}$ on DWI	0.083 (0.009–0.758)	0.028*	0.117 (0.027–0.502)	0.004*

Data are presented with the 95% confidence interval in parentheses

IPT inflammatory pseudotumor, *CLM* colorectal liver metastasis, *NA* not available, *AP* arterial phase, *TP* transitional phase, *T2WI* T2-weighted image, *HBP* hepatobiliary phase, *DWI*, diffusion-weighed image, $SIR_{lesion/liver}$ signal intensity ratio of lesion to liver

*$P < 0.05$

Table 4 Diagnostic ability for distinguishing IPT from CLM

	Cut-off value	Sensitivity	Specificity	LR+	LR−	AUC
$SIR_{lesion/liver}$ on HBP	0.52	87.1% (27/31)	82.4% (108/131)	4.96	0.16	0.895
$SIR_{lesion/liver}$ on DWI	2.45	90.3% (28/31)	88.5% (116/131)	7.89	0.11	0.907

Data are presented with numerators and denominators in parentheses

IPT inflammatory pseudotumor, *CLM* colorectal liver metastasis, $SIR_{lesion/liver}$ signal intensity ratio of lesion to liver, *HBP* hepatobiliary phase, *DWI* diffusion-weighed image, *LR+* positive-likelihood ratio, *LR−* negative-likelihood ratio, *AUC* area under the curve

respectively). Figures 4 and 5 present clinical cases of IPT and CLM.

Discussion

In our study, MRI of IPT had certain characteristic imaging features, including central hypointensity with a relatively hyperintense periphery on HBP and higher $SIR_{lesion/live}$ on HBP and lower $SIR_{lesion/live}$ on DWI than CLM. The discrimination ability of $SIR_{lesion/liver}$ on HBP and DWI were both high in IPT, which may be due to the abundant inflammatory cell infiltration in the center and concentrated fibrous tissue in the periphery of IPT lesions [6, 16]. Residual hepatocytes in the lesion can also play a role in relatively high signal intensity in IPT on HBP. The relatively lower DWI signal of IPT may be explained by the higher proton diffusivity due to edema than that of CLM.

Previous studies from Asian countries have reported that hepatic IPT was common in males in their late fifties [10, 17]. In this study, the male-to-female ratio was about 3:2 and the mean age was 59.3 years, which were similar to those reported previously.

According to previous reports, the enhancement pattern of IPT is variable, and includes mild enhancement on AP and marked enhancement on PVP, poorly defined rim enhancement on AP, or progressive hyperenhancement pattern with delayed rim enhancement [11, 15, 17–19]. The IPT mass shows mild enhancement on AP, probably due to its relatively low vascular supply from the hepatic artery, and distinct enhancement on PVP, as the peripheral area is composed of fibrillar collagen and is rich in capillaries. Delayed rim enhancement could correspond to the fibrous tissue in the periphery. The enhancement patterns are relevant to the course of the disease, presence of fibrous tissue, and cellular component, and therefore may vary. Previous reports have shown that T1-weighted images, T2WI, and dynamic CT findings are also nonspecific. Thus, it is difficult to make a correct preoperative diagnosis of IMT when using conventional imaging. Our results indicated that central hypointensity with a relatively hyperintense periphery on HBP and higher $SIR_{lesion/live}$ on HBP and lower $SIR_{lesion/live}$ on DWI were hallmark findings of IMT; therefore, gadoxetate disodium MRI may be helpful for distinguishing IPT from CLM.

There are several limitations in our study. First, we included clinically diagnosed IPT and CLM.

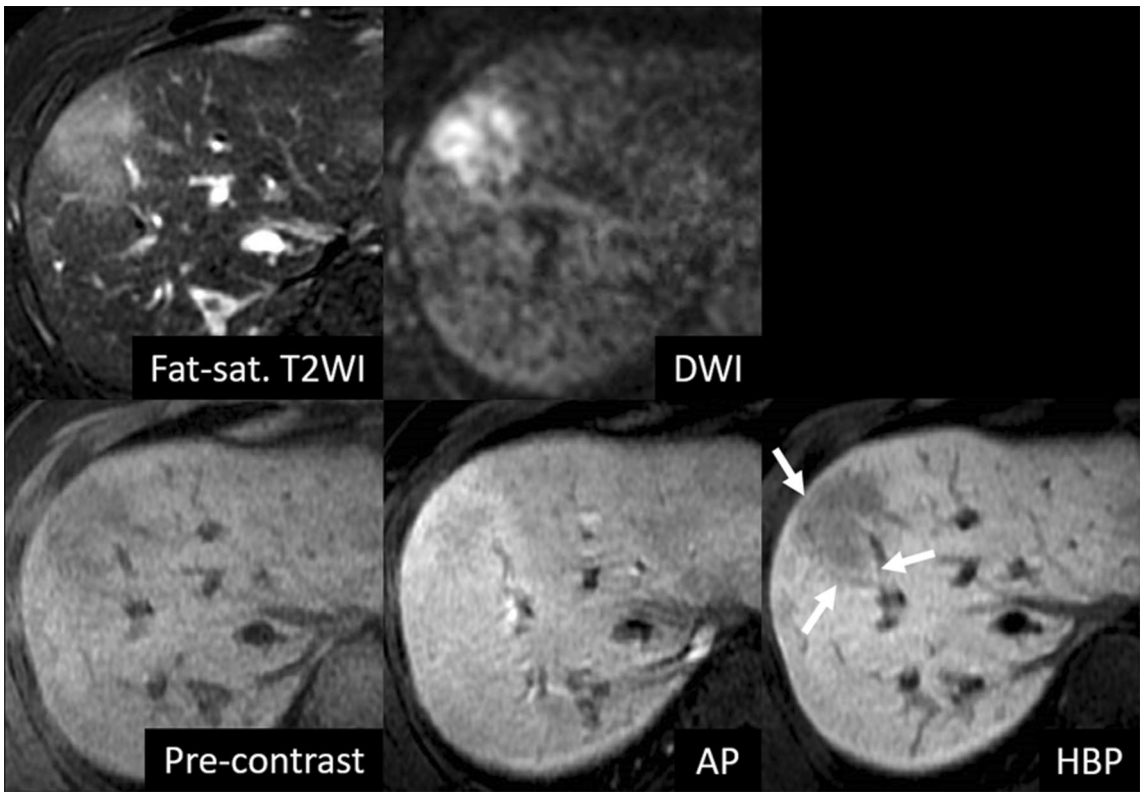

Fig. 4 A case with inflammatory pseudotumor (IPT). A 49-year-old man had IPT (35 mm) at S8. This lesion showed central hypointensity with a relatively hyperintense periphery on hepatobiliary phase (HBP) (arrows). The signal intensity ratio of the lesion to liver ($SIR_{lesion/liver}$) on HBP and DWI were 0.69 and 2.06, respectively. *Fat-sat.* fat-saturated, *T2WI* T2-weighted image, *DWI* diffusion-weighted image, *AP* arterial phase

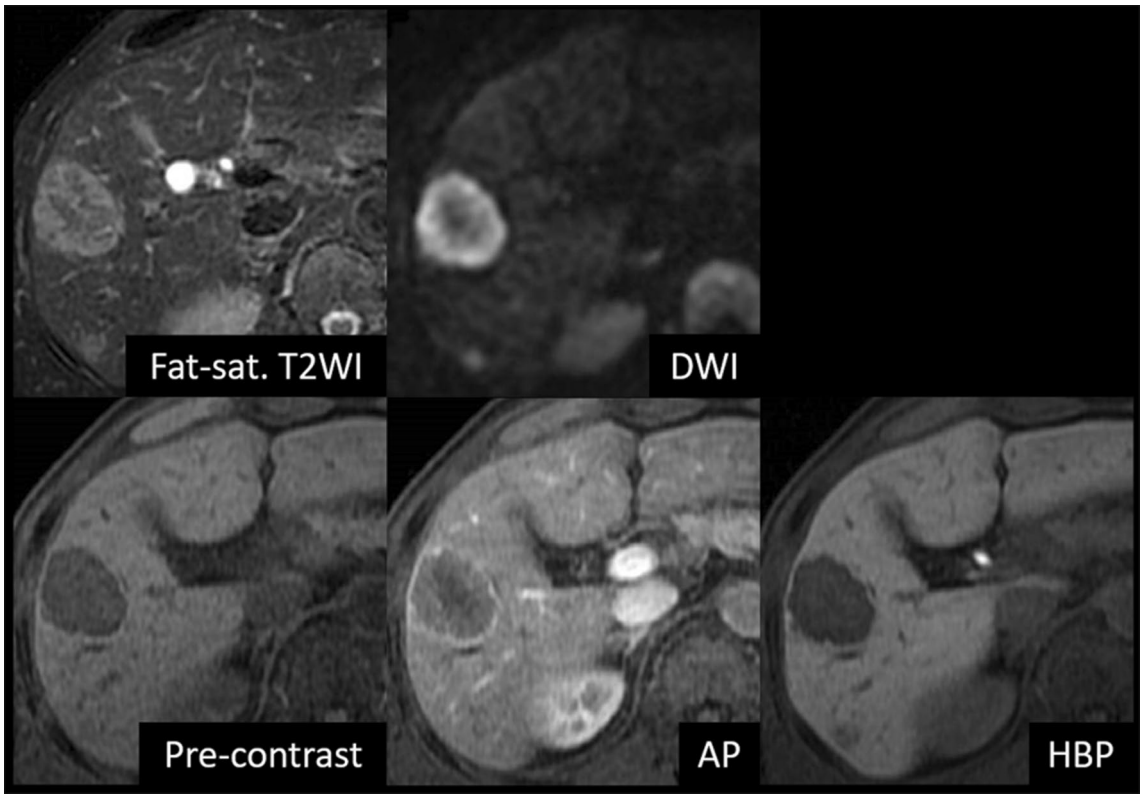

Fig. 5 A case with colorectal liver metastasis (CLM). A 73-year-old man had a CLM (39 mm) at S5. This lesion did not show central hypointensity with a relatively hyperintense periphery on the hepatobiliary phase (HBP). The signal intensity ratio of the lesion to liver ($SIR_{lesion/liver}$) on HBP and DWI were 0.46 and 3.63, respectively. *Fat-sat.* fat-saturated, *T2WI* T2-weighted image, *DWI* diffusion-weighted image, *AP* arterial phase

Histologically, IPT contains cells associated with both acute and chronic inflammation, including lymphocytes and plasma cells, myofibroblastic spindle cells, and collagen [1]. Our clinically diagnosed cases may not have had these characteristics, and our study population may have included a broad-sense ITP. In daily practice, it is difficult to obtain pathological confirmation for all ITPs; therefore, our findings are of clinical significance. Second, ITP was not classified into IgG4-related and non-IgG4-related cases in this study. Recently, evidence has indicated a close relationship between IgG4-related immune reactions and hepatic IPT [20, 21]. The two types differ not only in terms of their pathological characteristics, but also in the MRI findings obtained using extracellular contrast agent [17]. Third, the retrospective nature of and relatively small number of IPT cases in this study were also limitations. Further prospective studies with a larger sample size are necessary.

In summary, central hypointensity with a relatively hyperintense periphery on HBP and $SIR_{lesion/live}$ on HBP and DWI may be reliable gadoxetate disodium-enhanced MRI features for distinguishing IPT from CLM.

Funding This research received no specific Grant.

Compliance with ethical standards

Conflict of interest The authors declare that they have no conflict of interest.

References

1. Patnana M, Sevrukov AB, Elsayes KM, Viswanathan C, Lubner M, Menias CO (2012) Inflammatory pseudotumor: the great mimicker. AJR Am J Roentgenol 198:W217-W227. https://doi.org/10.2214/AJR.11.7288.
2. Matsuo Y, Sato M, Shibata T, et al (2014) Inflammatory pseudotumor of the liver diagnosed as metastatic liver tumor in a patient with a gastrointestinal stromal tumor of the rectum: report of a case. World J Surg Oncol 12:140. https://doi.org/10.1186/1477-7819-12-140.
3. Shirai Y, Shiba H, Fujiwara Y, Eto K, Misawa T, Yanaga K (2013) Hepatic inflammatory pseudotumor with elevated serum CA19-9 level mimicking liver metastasis from rectal cancer: report of a case. Int Surg 98:324-329. https://doi.org/10.9738/INTSURG-D-13-00091.1.
4. Ishida H, Tatsuta M, Furukawa H, et al (2000) Multiple inflammatory pseudotumors mimicking liver metastasis from colon cancer:

report of a case. Surg Today 30:530-533. https://doi.org/10.1007/s005950070121.
5. Bae SK, Abiru S, Kamohara Y, et al (2015) Hepatic inflammatory pseudotumor associated with xanthogranulomatous cholangitis mimicking cholangiocarcinoma. Intern Med 54:771-775. https://doi.org/10.2169/internalmedicine.54.2623.
6. Ahn KS, Kang KJ, Kim YH, et al (2012) Inflammatory pseudotumors mimicking intrahepatic cholangiocarcinoma of the liver; IgG4-positivity and its clinical significance. J Hepatobiliary Pancreat Sci 19:405-412. https://doi.org/10.1007/s00534-011-0436-z.
7. Iguchi H, Yamazaki H, Tsunoda H, Takahashi Y, Yokomori H (2013) A case of inflammatory pseudotumor of the liver mimicking hepatocellular carcinoma on EOB-MRI and PET. Case Rep Med 594254. https://doi.org/10.1155/2013/594254.
8. Yin L, Zhu B, Lu XY, Lau WY, Zhang YJ (2017) Misdiagnosing hepatic inflammatory pseudotumor as hepatocellular carcinoma: A case report. JGH Open 1:76-78. https://doi.org/10.1002/jgh3.12012.
9. Ananthakrishnan A, Gogineni V, Saeian K (2006) Epidemiology of primary and secondary liver cancers. Semin Intervent Radiol 23:47-63. https://doi.org/10.1055/s-2006-939841.
10. Park KS, Jang BK, Chung WJ, et al (2006) Inflammatory pseudotumor of liver--a clinical review of 15 cases. Korean J Hepatol 12:429-438.
11. Park JY, Choi MS, Lim YS, et al (2014) Clinical features, image findings, and prognosis of inflammatory pseudotumor of the liver: a multicenter experience of 45 cases. Gut Liver 8:58-63. https://doi.org/10.5009/gnl.2014.8.1.58.
12. Moon JY, Kim SH, Choi SY, Hwang JA, Lee JE, Lee J (2018) Differentiating malignant from benign hyperintense nodules on unenhanced T1-weighted images in patients with chronic liver disease: using gadoxetic acid-enhanced and diffusion-weighted MR imaging. Jpn J Radiol 36:489-499. https://doi.org/10.1007/s11604-018-0748-x.
13. Asato N, Tsurusaki M, Sofue K, et al (2017) Comparison of gadoxetic acid-enhanced dynamic MR imaging and contrast-enhanced computed tomography for preoperative evaluation of colorectal liver metastases. Jpn J Radiol 35:197-205. https://doi.org/10.1007/s11604-017-0622-2
14. Choi SH, Lee SS, Park SH, et al (2019) LI-RADS Classification and Prognosis of Primary Liver Cancers at Gadoxetic Acid-enhanced MRI. Radiology 290:388-397. https://doi.org/10.1148/radiol.2018181290.
15. Chang AI, Kim YK, Min JH, Lee J, Kim H, Lee SJ (2019) Differentiation between inflammatory myofibroblastic tumor and cholangiocarcinoma manifesting as target appearance on gadoxetic acid-enhanced MRI. Abdom Radiol 44:1395-1406. https://doi.org/10.1007/s00261-018-1847-y
16. Chang SD, Scali EP, Abrahams Z, Tha S, Yoshida EM (2014) Inflammatory pseudotumor of the liver: a rare case of recurrence following surgical resection. J Radiol Case Rep 8:23-30. https://doi.org/10.3941/jrcr.v8i3.1459.
17. Sheng RF, Zhai CW, Ji Y, Chen CZ, Yang L, Zeng MS (2017) Role of MR in the differentiation of IgG4-related from non-IgG4-related hepatic inflammatory pseudotumor. Hepatobiliary Pancreat Dis Int 16:631-637. https://doi.org/10.1016/S1499-3872(17)60062-6.
18. Ijuin H, Ono N, Koga K, et al (1997) Inflammatory pseudotumor of the liver--MR imaging findings. Kurume Med J 44:305-313. https://doi.org/10.2739/kurumemedj.44.305
19. Xiao Y, Zhou S, Ma C, Luo J, Zhu H, Tang F (2013) Radiological and histopathological features of hepatic inflammatory myofibroblastic tumour: analysis of 10 cases. Clin Radiol 68:1114-1120. https://doi.org/10.1016/j.crad.2013.05.097.
20. Zen Y, Fujii T, Sato Y, Masuda S, Nakanuma Y (2007) Pathological classification of hepatic inflammatory pseudotumor with respect to IgG4-related disease. Mod Pathol 20:884-894. https://doi.org/10.1038/modpathol.3800836.
21. Yamamoto H, Yamaguchi H, Aishima S, et al (2009) Inflammatory myofibroblastic tumor versus IgG4-related sclerosing disease and inflammatory pseudotumor: a comparative clinicopathologic study. Am J Surg Pathol 33:1330-1340. https://doi.org/10.1097/pas.0b013e3181a5a207